Brillouin light scattering during shearing of complex fluids

CLAUDIUS MORITZ LEHR,[1,2] OLGA ASTASHEVA,[1] AND JÖRG BALLER[1,3] (ID)

[1]*Department of Physics & Materials Science, University of Luxembourg, 1511 Luxembourg, Luxembourg*
[2]*claudiusmoritz.lehr@uni.lu*
[3]*joerg.baller@uni.lu*

Abstract: A setup for the optical measurement of elastic properties during the flow of complex fluids is presented. Brillouin light scattering and rotational rheology are combined in order to simultaneously measure the high-frequency longitudinal elastic modulus in a classical rheometer along with the zero-shear viscosity. Brillouin light scattering allows for the contactless determination of local elastic properties. First measurements of a diluted polymer system suggest a homogeneous orientation of polymer molecules throughout the sample as soon as a critical shear rate has been reached at one spatial position.

1. Introduction

When complex fluids are subject to shear flow, many different phenomena such as orientation of molecules or fillers, nucleation of crystals, shear banding etc. can occur. There exist optical techniques like particle image velocimetry (PIV), polarizing microscopy or dynamic light scattering which give access to structural or dynamic information [1,2]. It would be desirable to have a technique which would deliver information about mechanical properties on a microscopic scale during shearing of complex fluids. Brillouin light scattering (BLS) is such a contactless, non-destructive technique to measure elastic moduli at high frequencies using an optical spectrometer. It exploits scattering of light at thermal phonons. The propagation velocity of the thermally activated longitudinal or transversal sound waves delivers direct information on the effective spring constants for this type of propagating modes. Using different experimental setups, it is in principle possible to derive the complete elastic stiffness tensor with a spatial resolution which is only limited by the optical setup used [3]. In order to investigate the influence of shear flow on complex fluids, rotational rheology is widely used [4]. It is a very common technique to macroscopically measure elastic susceptibilities such as complex viscosities and shear moduli and study nonlinear behavior such as shear thinning occurring in complex fluids [5,6]. Rotational rheology delivers indirect information about shear induced alignment on different length scales (from fillers to molecular order) or shear induced crystallization. For a more detailed study of the influence of shearing on complex fluids, rheology has e.g. been coupled with polarizing microscopy and different small-angle scattering technologies: SALS, SAXS, SANS [2,7–15]. Part of these techniques are able to deliver spatially resolved information.

The main objective of this work is the development of an experimental setup which allows to use an optical method to locally record elastic moduli at high frequencies during the shear flow of complex fluids. A technique is presented to apply BLS inside the gap of a rotational rheometer. The longitudinal stiffness tensor which is related [16,17] to Young's modulus is determined by BLS and compared to the zero-shear viscosity measured by classical rotational rheology at the same time. The setup which is described here in detail is limited to one single scattering geometry thus only delivering one component, the longitudinal rigidity modulus (M'), of the elastic stiffness tensor. This study aims at being the start for the development of

more sophisticated setups allowing the record of the complete stiffness tensor at hypersound frequencies during shearing of complex fluids.

2. Experimental

2.1. Materials

For the demonstration of the new experimental technique, a transparent, nontoxic and easy-to-handle sample has been chosen, which shows shear thinning and exhibits a good scattering cross section. The polymer polyvinylpyrrolidone (PVP1300000 from Sigma Aldrich) with an average molecular mass of 1300000 g/mol has been diluted with polyethylene glycol (PEG400 from Carl Roth) with a molecular mass of 380-420 g/mol as solvent. The polymer and the solvent were first shortly mixed using a tilt/roller mixer at room temperature and then treated with a magnet stirrer at 70°C for 24 hours. The result is a transparent sample with a PVP1300000 concentration of 2.5 wt. %. Air bubbles due to the mixing process have been removed by applying vacuum.

For the evaluation of elastic moduli from Brillouin spectra, the knowledge of the mass density and the refractive index of the polymer solution is required. Figure 1 shows the temperature dependency of these two quantities measured with a density meter (5000M from Anton Paar) and a refractometer (Abbemat-WR from Anton Paar).
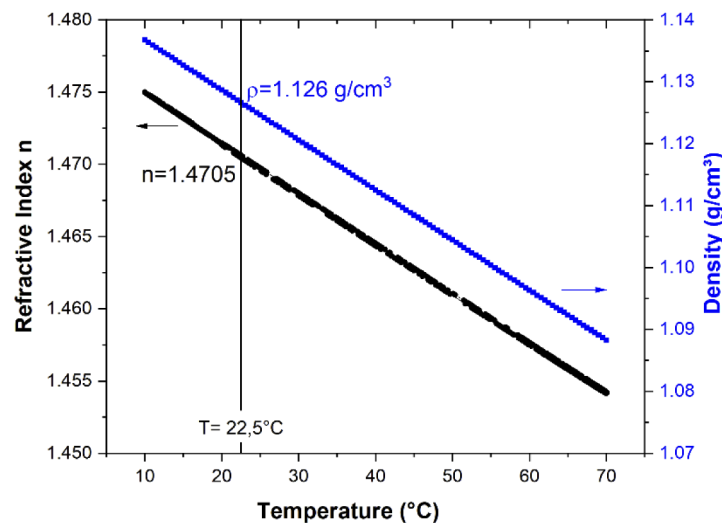

Fig. 1. Temperature dependence of the density and the refractive index (at a wavelength of 532 nm).

2.2. Rheology

Rheology has been performed with a rotational rheometer MCR302 (from Anton Paar) using plate-plate geometry [6] with a gap size of H=0.5 mm (Fig. 2). The upper plate (PP25) has a diameter of 25 mm. Plate/plate geometry has been chosen to be ready for more advanced scattering geometries using a polished upper plate as a mirror (to be published). For the optical access to the sample stage a temperature-controlled glass bottom plate (P-PTD200/GL from Anton Paar) has been installed. The position of the scattering volume for Brillouin spectroscopy is schematically indicated in Fig. 2 (red star).

During the experiments shown in this work, the viscosity of the samples has been recorded as a function of the shear rate (flow curves). With plate-plate geometries, the shear field inside the sample is nonhomogeneous. Therefore, the shear stress or shear rate is an average value the
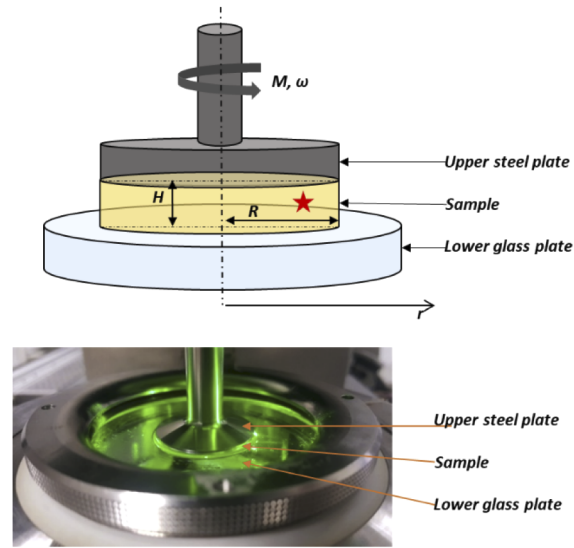
Fig. 2. Top, Illustration of the plate-plate geometry; red star: Position of the scattering volume for the Brillouin measurements. Bottom: Picture of the sample stage with laser turned on.

rheometer can be set to. The rheometer software calculates, according to the used geometry, a value for the dynamic viscosity η by the given shear stress τ for a given shear rate $\dot{\gamma}$ [6,18]

$$\eta = \frac{\tau}{\dot{\gamma}} \qquad (1)$$

The rheological measurements are macroscopic measurements whereas Brillouin spectroscopy measures local mechanical properties. i.e. the value of the shear rate at the position of the scattering volume must be known.

Depending on the torque M measured by the rheometer, the shear stress at the radial position r ($r=0..R$) can be formulated as follows (see Fig. 2)

$$\tau = \frac{2M}{\pi * r^3} \qquad (2)$$

The local shear rate at a position r depends on the angular velocity applied by the rheometer and the gap size H [6]:

$$\dot{\gamma} = \frac{\omega * r}{H} \qquad (3)$$

2.3. Influence of plate diameter and material

In order to experimentally determine the range of shear rates for which reliable data can be recorded with the 25 mm steel top plate (PP25), measurements with a larger top plate (GL43-HT, R=43 mm) have been performed (Fig. 3). Consequently, only data points recorded at shear rates higher than 10 s^{-1} will be discussed in the following. By using a top plate made out of glass (GL25-BK7), it could be confirmed (also shown in Fig. 3) that for these experiments, the plate material has no influence on the results. In the following, only measurements using the PP25 steel plate are discussed.
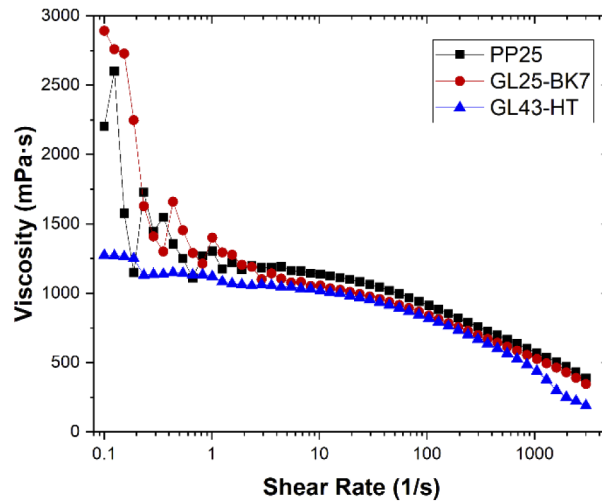
Fig. 3. Flow curves measured with different top plates. Black squares: PP25 (steel, R = 25 mm). Red circles: GL25-BK7 (glass, R=25 mm). Blue triangles: GL43-HT (glass, R=43 mm). Temperature: 22.5°C.

2.4. Control of temperature

To control the temperature in the sample more precisely, a hood (H-PTD200 from Anton Paar) has been installed, see Fig. 4. The hood is purged with air at a flow rate of 180 l/h. The temperature control could be influenced by modifications of the housing of the MCR302 rheometer necessary to gain optical access. In order to find the conditions for reliable temperature measurements, a PT100 temperature probe has been introduced into the sample (Fig. 4).
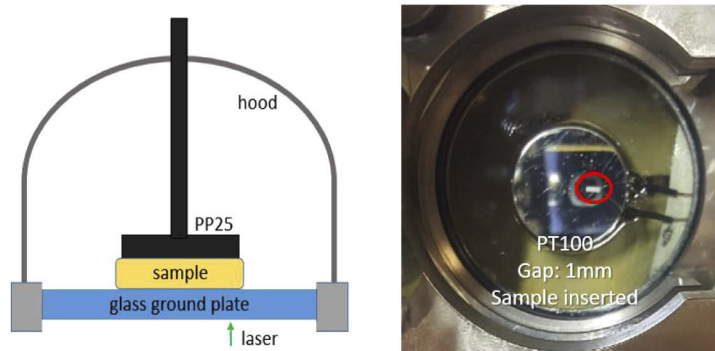

Fig. 4. Left, illustration of the sample stage with H-PTD200 hood. Right, view of the sample stage from below. The top plate PP25 is set at a gap size of 1 mm to the lower glass plate. The transparent sample with the additional temperature sensor (marked with red circle) is in between.

Figure 5 shows an overview of the dependencies of two measured temperatures from the set temperature. It turns out that the sample temperature differs from the temperature indicated by the rheometer software and that a waiting time of about 20 minutes is needed to guarantee steady conditions in the temperature range used. Therefore, for all measurements presented here, a correction of the temperature indicated by the rheometer software has been done and a waiting time of 20 minutes after changing the sample temperature has been respected. All rheological

measurements have been performed without the PT100 temperature probe and with a gap size of 0.5 mm.
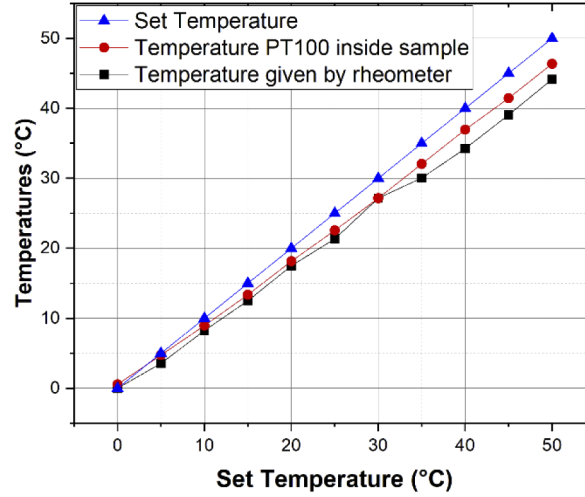

Fig. 5. Comparison of temperatures. Blue triangles: Set temperature in the rheometer software. Black squares: Temperature measured inside the sample after the rheometer control indicates a stable temperature. Red circles: Temperature measured inside the sample after 20 minutes.

2.5. Brillouin spectroscopy

Brillouin spectroscopy is a non-contact method to determine elastic properties of materials with optical means. The scattering of light at thermal phonons (Brillouin scattering) was first postulated by Léon Brillouin [19] in 1922. For this inelastic scattering process, conservation of energy and momentum holds [20]:

$$\hbar\omega_s^{\pm} = \hbar\omega_i \pm \hbar\Omega$$
$$\vec{k}_s^{\pm} = \vec{k}_i \pm \vec{q} \tag{4}$$

with ω_i, $\vec{k}_i$: angular frequency and wave vector of the incident light, ω_s, $\vec{k}_s$: angular frequency and wave vector of the scatter light, Ω, $\vec{q}$: angular frequency and wave vector of the phonon. The ± denotes annihilation and creation of phonons (stokes and anti-stokes scattering) for an inelastic scattering process where the frequency shift of the scattered light is positive or negative.

For isotropic samples, the wave vector of the acoustic phonon depends on the scattering angle θ_i (see Fig. 6), the refractive index n of the sample and the wave length λ_0 of the laser (532 nm) [21]:

$$q = \frac{4\pi n * \sin\left(\frac{\theta}{2}\right)}{\lambda_0} \tag{5}$$

For the Brillouin measurements presented her, backscattering ($\theta = 180°$) has been used. So, the relation reduces to the following expression for the acoustic wave vector q^{180} for back

scattering:

$$q^{180} = \frac{4\pi n}{\lambda_0} \tag{6}$$

with $q^{180} = \frac{\omega^{180}}{v^{180}}$ it follows for the dependency of the sound velocity v^{180} from the measured Brillouin shift $f^{180} = \frac{\omega^{180}}{2\pi}$ in the spectra:

$$v^{180} = \frac{f^{180}\lambda_0}{2n} \tag{7}$$

In the backscattering geometry applied here, only the frequencies of the longitudinal phonons (see also next paragraph) could be evaluated. From the sound velocity of the longitudinal phonons v_{long} in an isotropic medium, the longitudinal rigidity modulus M' can be calculated using the data from the density measurements (Fig. 1):

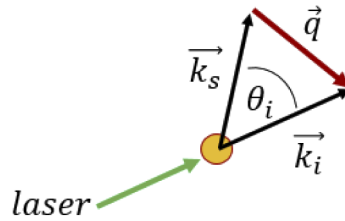$$M' = \rho v_{long}^2 \tag{8}$$

Fig. 6. Inelastic scattering process.

It follows finally for M' [22]:

$$M' = \rho \left(\frac{f^{180}\lambda_0}{2n} \right)^2 \tag{9}$$

A Sandercock-type Fabry-Perot Interferometer (TFP-2 HC from Table Stable LTD) has been used to record Brillouin spectra. An optically pumped semiconductor laser (Verdi-G2 Series from Coherent) with a wavelength of 532 nm has been used as light source. The spectra have been recorded with an acquisition time of about 4 minutes for the temperature dependent measurements shown in Fig. 11, 15 minutes for the shear rate dependent measurements (Fig. 12) and 50 seconds for the relaxation measurements (Fig. 13).

2.6. Spectrum analysis

The Brillouin spectra have been evaluated using the Damped Harmonic Oscillator (DHO) model. The Brillouin line widths are directly linked to the longitudinal viscosity (at hypersound frrequencies) which makes its evaluation of great use. Since the changes of the spectra due to different temperatures or shear rates are very small, evolution of the DHO line widths unfortunately does not yield reliable information–at least for the current setup. This is illustrated in Fig. 7. It shows the line width data for the temperature dependent measurements in Fig. 11.

The same holds true for the line widths of the measurements depicted in Fig. 12 and 13. Therefore, line widths are not discussed in the following.

2.7. Combination of rheology and Brillouin scattering

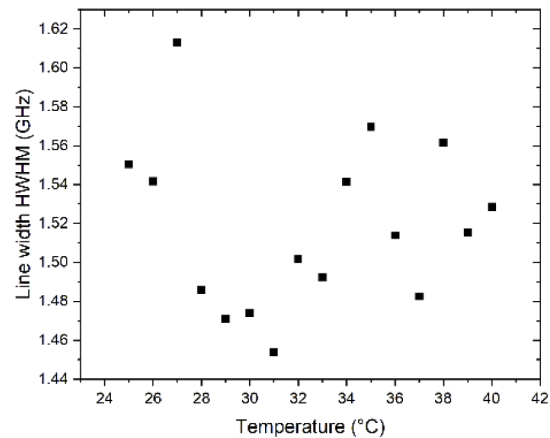The experimental set-up for the combination of rheology and Brillouin scattering is shown in Fig. 8.

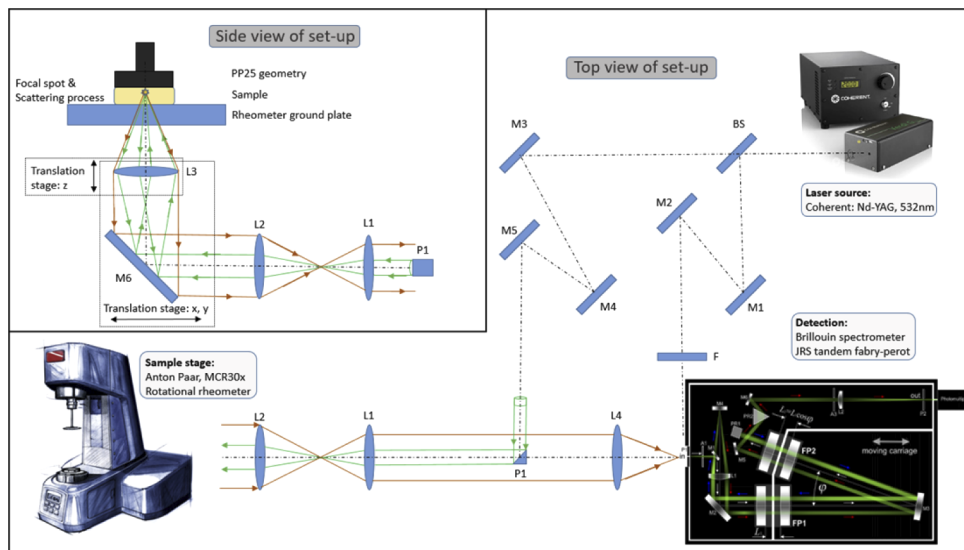**Fig. 7.** Line width from DHO fits for the measurement shown in Fig. 11.

Fig. 8. Illustration of the experimental set-up. The main components are the laser light source (532 nm), the rotational rheometer (MCR302 from Anton Paar) as sample stage and the tandem Fabry-Perot spectrometer to probe Brillouin scattering. BS: beam-splitter, M: mirrors, F: intensity filter, P: prism and L: lenses. For more information, see text.

For more details on the optical setup typically used for Brillouin scattering please refer to [21,23]. The main part of the laser beam is directed onto prism P1 used to implement 180° backscattering geometry. The beam is expanded with telescope optics (lenses L1 and L2) to reach smaller focal parameters. Mirror M6 reflects the expanded beam up to the rheometer sample stage. In front of the ground glass plate of the rheometer`s sample stage an objective lens L3 is positioned. It is mounted on a translation stage in order to be able to move the focal point along the optical axis (see below). In order to exclude direct reflections from the different optical surfaces in the rheometer setup, the incoming laser beam (green lines) is slightly tilted by 4° with respect to the surface normal of the rheometer plates. The detection path, indicated with red lines starts from the scattering volume and collects with the objective lens L3 the scattered

light and leads it over the prism (which cuts out a part) to the ocular lens L4 which projects it onto the entry slit of the spectrometer. The small angle of 4° with respect to the surface normal diminishes the effect of potential optical birefringence due to shear induced orientation.

2.8. Dimensions of the scattering volume

Regarding the sample thickness of 0.5 mm (given by the gap between the rheometer plates), the dimensions of the scattering volume should be just a fraction of this value in order to be able to move it freely inside the sample volume. As the chosen sample thickness is 500 µm the focal spot should have a max. dimension of about 50 µm. For a Gaussian beam the radius of a focal spot is [24]

$$\omega_0 = \frac{\lambda}{\pi * k * \Theta} \tag{10}$$

where λ is the wavelength, k the beam quality factor ($1 < k < 1.1$ for the Verdi G2) and Θ the angle of the beam's edges to focus on the optical axis:

$$\Theta = \arctan\left(\frac{\omega_{ObjL}}{f_{ObjL}}\right) \tag{11}$$

with ω_{ObjL} the beam radius of the beam approaching the focusing (objective) lens and f_{ObjL} the focal length of it as illustrated in Fig. 9.
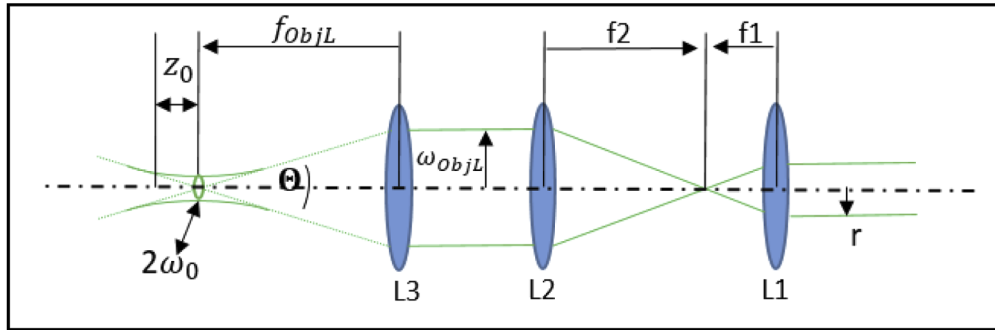

Fig. 9. Illustration of the focal spot parameters (left) and the telescope beam expanding optics (right).

The focal spot radius can then be expressed as

$$\omega_0 = \frac{\lambda * f_{ObjL}}{\pi * k * \omega_{ObjL}} \tag{12}$$

the corresponding focal length:

$$z = 2 * z_0 = 2 * \frac{(k * \pi * \omega_0^2)}{\lambda} \tag{13}$$

Prism P1 has a reflecting area with the dimension of 3 mm*4.2 mm whereas the given laser beam radius is 2.3 mm, so the maximum radius of the beam after the prism is about 1.5 mm (r in Fig. 9) A widening of the beam diameter is required to achieve smaller focal parameters. Two lenses (telescope optics L1 and L2) are set in front of the objective lens (L3). Due to the 1" optics used in the setup the aperture of the lenses is limited to 25.4 mm. The beam radii and

focal lengths are illustrated in Fig. 9 and the relation between them can be formulated as follows:

$$R = r * \frac{f_2}{f_1} \tag{14}$$

The combination of f=25.4 mm optics (L1) and f=140 mm (L2) gives a beam radius ω_{ObjL} of 6.2 mm which corresponds to a diameter of 12.4 mm and fits the condition. Having the maximum beam radius before focusing and the minimal focusing length of 60 mm for the objective lens (due to construction of the rheometer) as well as the laser beam parameters of quality (k=1.05) an estimation of the focal length can be given as follows:

$$
\begin{aligned}
z_0 &= \frac{\lambda * f^2}{\pi * k} * \frac{1}{\omega_{ObjL}^2} \\
&= \frac{1}{\omega_{ObjL}^2} * \frac{532 * (10^{-9})m * 0.06^2 m^2}{\pi * 1.05} \\
&= \left(\frac{1}{\omega_{ObjL}^2(m^2)} * 0.58059 * 10^{-9} \, m^3 \right)
\end{aligned}
\tag{15}
$$

Equation (15) can be used to calculate the focal spot length for the used set-up by setting the beam radius ω_{ObjL} before focusing. This leads to a focal length z=2*z_0 of 32 μm for a beam radius of 6 mm before focusing which is sufficient for the following experiments. The corresponding focal diameter $2\omega_0$ is 3.2 μm. For the measurements presented here, no slit or pinhole has been used in the setup shown in Fig. 9. Therefore, the focal length of 32 μm is not equal to the dimensions of the scattering volume. It moreover indicates the region where most of the information is gathered. The samples investigated are expected to show heterogeneities due to shear induced structuring on length scales far below the phonon wave length. Therefore we do not expect a falsification of phonon frequencies by the fact that Eq. (6) no longer holds as; e.g., discussed in [25].

2.9.   Identification of the scattering volume

As shown in Fig. 8 the scattering volume can be shifted vertically between the rheometer plates by moving lens L3. In order to calibrate the position of the scattering volume, Brillouin spectra have been recorded for different vertical positions z of the scattering volume. Figure 10 shows the measured Brillouin frequency shifts as well as the signal height as a function of z–both for no shear ($\dot{\gamma} = 0 \, \text{s}^{-1}$) and shear ($\dot{\gamma} = 3000 \, \text{s}^{-1}$).

Even when the scattering volume lies mainly outside the sample; e.g., mainly in the lower glass plate, the Brillouin frequencies attributed to the smaller sample volume remain the same. The Brillouin frequencies for the glass plates lie outside the chosen free spectral range of the spectrometer. Therefore, the frequency shifts give no precise information about the position of the scattering volume [Fig. 10 (left)]. In contrast to this, the signal height is directly proportional to the amount of sample material which lies inside the scattering volume. Therefore, evaluation of the signal heights allows to ensure a more precise positioning of the focal spot in z-direction. For the measurements discussed in this work, the focal position is set to the middle of the gap between the rheometer plates. It should be emphasized that the application of shear has no influence on the signal heights and the position of the scattering volume [Fig. 10 (right)]. The recorded frequencies [Fig. 10 (left)] differ with and without shear which is a first indication that Brillouin scattering is sensitive to shear thinning (please see below for a detailed discussion).
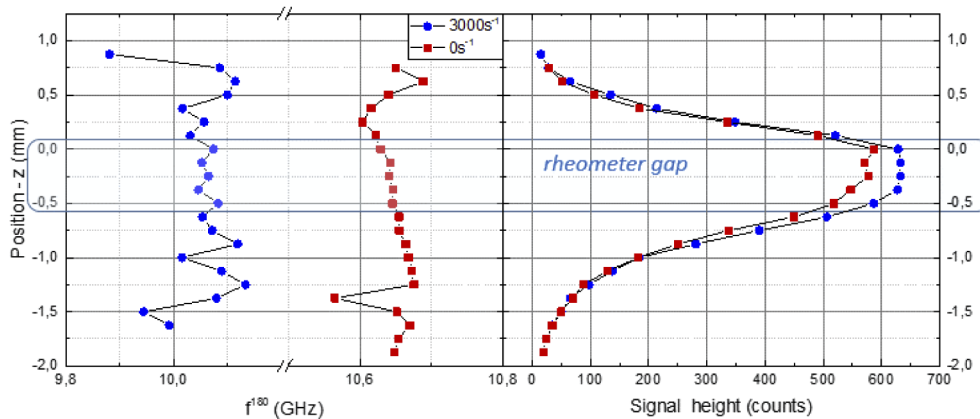
Fig. 10. Brillouin measurements during vertical movement of the scattering volume. (left) Brillouin frequencies f^{180} . (right) Corresponding signal height.

3. Measurements with the new setup and discussion

As a first test of the combined setup, a simultaneous rheology and Brillouin scattering measurement as a function of temperature at constant shear rate $\dot{\gamma}=3000$ s^{-1} has been performed. Figure 11 shows η measured by rheology (macroscopic value) and M' [Eq. (9)] measured by Brillouin spectroscopy (scattering volume near the edge of the rheometer plates as indicated in the upper part of Fig. 2). As expected, both elastic susceptibilities diminish with increasing temperature. It should be emphasized that the viscosity reflects the answer of the system to pure shearing whereas M' is the susceptibility related to a purely longitudinal elongation [22]. Moreover, the viscosity is a quasi-static quantity whereas the longitudinal modulus has been measured at frequencies in the GHz range where the system is dynamically clamped. As discussed in the introduction, the modulus measured by Brillouin spectroscopy at high frequencies detects the effective "spring constants" which determine the propagation of the longitudinal, thermally induced sound waves. It also contains the temperature dependency of the mass density [see Eq. (9)].

The temperature dependent measurement shown in Fig. 11 shows that both elastic suscep-tibilities show a similar behavior. We must emphasize that there is no direct causal relation between both susceptibilities. Figure 11 demonstrates that the temperature dependency of both susceptibilities can be resolved by the presented setup. The combined technique shall now be applied to a measurement where the shear rate is varied in the range where shear thinning can be detected for the system under study.

The flow curve (filled black circles in Fig. 12) depict the shear thinning behavior expected for the diluted polymer system.

Shear thinning is visible in the whole range of shear rates applied.

The elastic modulus M' (open symbols in Fig. 12) shows a softening only at shear rates higher than 500 s^{-1}. It can only be speculated if this is due to the fact that the q-vector of the longitudinal wave is perpendicular to the normal of the rheometer plates and that ordering of molecules parallel to the rheometer plates occurs only at higher shear rates. This interesting scenario can be investigated with an improved setup (under development) which allows to record all components of the elastic stiffness tensor by using different scattering geometries.

The most surprising result from the investigations with Brillouin spectroscopy can be seen when comparing measurements of M' at different radial positions r (see Fig. 2) in the gap between the rheometer plates. The three curves (open symbols in Fig. 12) are measurements of M' at the center (r=0.5 mm, red squares); at the middle (r=6.5 mm, green triangles) and near the
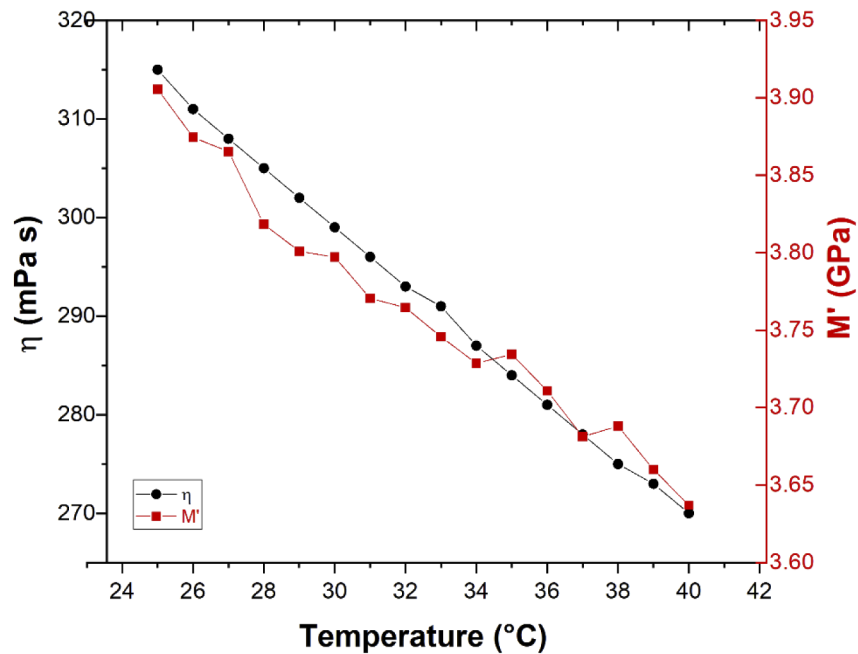
Fig. 11. Simultaneous measurement of η and M′ as a function of sample temperature. Shear rate $\dot{\gamma}$=3000 s^{-1}. The scattering volume of the Brillouin measurements is situated close to the edge of the rheometer plates as shown in the upper part of Fig. 2.
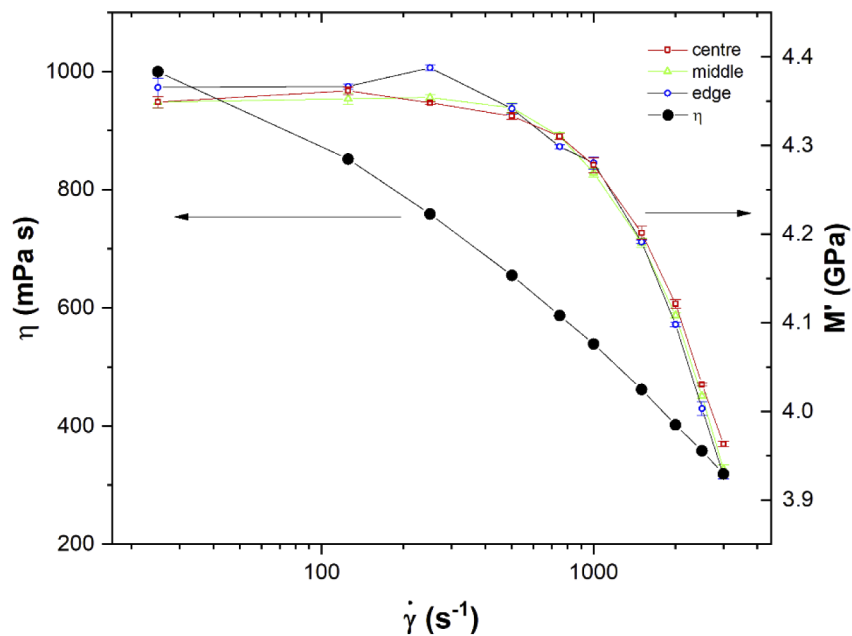

Fig. 12. Viscosity and elastic moduli at different radial positions as a function of shear rate. The lines are guidelines to the eyes.

border of the plate/plate geometry (r=12.5 mm, blue circles). All measurements show nearly the same dependency on the shear rate. This means that when the shear thinning, i.e. orientation of molecules starts at the extremities of the rheometer plates where the local shear rate has the highest values [see Eq. (3)], it influences also the parts of the sample with locally lower shear rates. If this effect is due to a different influence of the molecular orientation on the hyper sound modulus than to the quasi-static viscosity deserves further investigations. In order to confirm that the observed softening of M' is due to shear induced orientation, the following experimental procedure has been applied: the sample has been sheared at a shear rate of 3000 s^{-1} for 20 minutes. Then the rheometer has been stopped and Brillouin spectra have been recorded over a time span of 20 minutes.

Figure 13 shows that the modulus M' relaxes almost completely back to the value at the start of the experiment shown in Fig. 12 at $\dot{\gamma}$=0 s^{-1}. This is a confirmation of the assumption that the shear induced change of M' recorded by Brillouin scattering has its origin in structural changes.
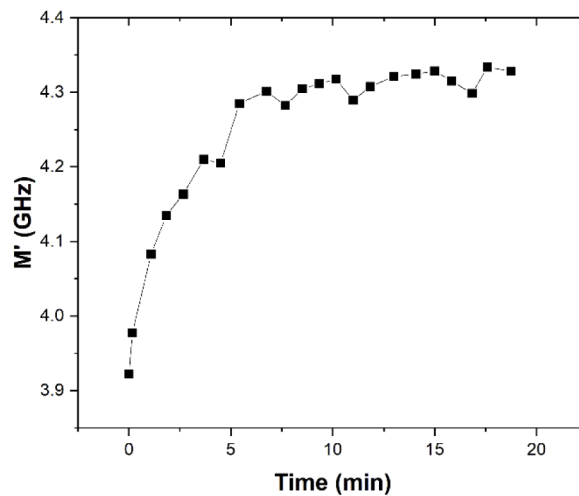

Fig. 13. M' measured for 20 minutes with the rheometer at rest after shearing with $\dot{\gamma} = 3000$ s^{-1}.

4. Conclusions and outlook

The combination of classical rotational rheology and Brillouin light scattering could be successfully demonstrated. Temperature dependent measurements yielded a similar behavior of the viscosity and the hypersound modulus. Shear thinning is also depicted by both mechanical susceptibilities. Brillouin scattering offers the advantage of being a local probe of elastic properties. The shear thinning evidenced by the hypersound modulus suggests that shear induced alignment simultaneously occurs throughout the sample even when the local shear rate varies as this is the case in the plate/plate geometry.

Based on the current work, measurements with different (rheometer) geometries (especially cone/plate geometry) and different light scattering geometries are expected to deliver the full elastic tensor with a spatial resolution of about 50 µm inside the gap of a rotational rheometer. It is expected to shed more light on local causes of shear thinning, shear banding etc.

References

1. K. I. W. Kane, E. L. Moreno, C. M. Lehr, S. Hachi, R. Dannert, R. Sanctuary, C. Wagner, R. M. T. Fleming, and J. Baller, "Determination of the rheological properties of Matrigel for optimum seeding conditions in microfluidic cell cultures," AIP Adv. **8**(12), 125332 (2018).
2. G. G. Fuller, *Optical rheometry of complex fluids* (Oxford Press, 1995).
3. J. Baller, J. K. Kruger, R. Birringer, and C. Proust, "Elastic properties of single-crystalline and consolidated nano-structured yttrium oxide at room temperature," J. Phys.: Condens. Matter **12**(25), 5403–5409 (2000).
4. A. Deshpande, J. M. Krishnan, and P. B. Kumar, *Rheology of complex fluids* (Springer, New York, 2010).
5. H. Janeschitz-Kriegl, *Polymer Melt Rheology and Flow Birefringence*, Polymers - Properties and Applications (Springer, Berlin Heidelberg, 1983).
6. C. W. Macosko, "*Rheology. Principles, Measurements and Applications*," (VCH, New York, 1994).
7. R. H. Somani, L. Yang, B. S. Hsiao, P. K. Agarwal, H. A. Fruitwala, and A. H. Tsou, "Shear-induced precursor structures in isotactic polypropylene melt by in-situ rheo-SAXS and rheo-WAXD studies," Macromolecules **35**(24), 9096–9104 (2002).
8. A. M. Philippe, C. Baravian, M. Imperor-Clerc, J. De Silva, E. Paineau, I. Bihannic, P. Davidson, F. Meneau, P. Levitz, and L. J. Michot, "Rheo-SAXS investigation of shear-thinning behaviour of very anisometric repulsive disc-like clay suspensions," J. Phys.: Condens. Matter **23**(19), 194112 (2011).
9. T. Meins, K. Hyun, N. Dingenouts, M. F. Ardakani, B. Struth, and M. Wilhelm, "New Insight to the Mechanism of the Shear-Induced Macroscopic Alignment of Diblock Copolymer Melts by a Unique and Newly Developed Rheo-SAXS Combination," Macromolecules **45**(1), 455–472 (2012).
10. T. Kume, T. Hashimoto, T. Takahashi, and G. B. Fuller, "Rheo-optical studies of shear-induced structures in semidilute polystyrene solutions," Macromolecules **30**(23), 7232–7236 (1997).
11. P. Van Puyvelde, H. Yang, J. Mewis, and P. Moldenaers, "Rheo-optical probing of relaxational phenomena in immiscible polymer blends," J. Colloid Interface Sci. **200**(1), 86–94 (1998).
12. H. Yang, H. J. Zhang, P. Moldenaers, and J. Mewis, "Rheo-optical investigation of immiscible polymer blends," Polymer **39**(23), 5731–5737 (1998).
13. A. P. R. Eberle and L. Porcar, "Flow-SANS and Rheo-SANS applied to soft matter," Curr. Opin. Colloid Interface Sci. **17**(1), 33–43 (2012).
14. L. T. Andriano, N. Ruocco, J. D. Peterson, D. Olds, M. E. Helgeson, K. Ntetsikas, N. Hadjichristidis, S. Costanzo, D. Vlassopoulos, R. P. Hjelm, and L. G. Leal, "Microstructural characterization of a star-linear polymer blend under shear flow by using rheo-SANS," J. Rheol. **64**(3), 663–672 (2020).
15. O. O. Mykhaylyk, N. J. Warren, A. J. Parnell, G. Pfeifer, and J. Laeuger, "Applications of shear-induced polarized light imaging (SIPLI) technique for mechano-optical rheology of polymers and soft matter materials," J. Polym. Sci. Part B: Polym. Phys. **54**(21), 2151–2170 (2016).
16. R. Prevedel, A. Diz-Munoz, G. Ruocco, and G. Antonacci, "Brillouin microscopy: an emerging tool for mechanobiology," Nat. Methods **16**(10), 969–977 (2019).
17. F. Palombo and D. Fioretto, "Brillouin Light Scattering: Applications in Biomedical Sciences," Chem. Rev. **119**(13), 7833–7847 (2019).
18. G. Schramm, "A Practical Approach to Rheology and Rheometry."
19. L. Brillouin, "Diffusion de la lumière et des rayons X par un corps transparent homogène," Ann. Phys. **9**(17), 88–122 (1922).
20. J. G. Dil, "Brillouin-scattering in condensed matter," Rep. Prog. Phys. **45**(3), 285–334 (1982).
21. J.-K. Krüger, "Brillouin Spectroscopy and its Application to Polymers," in *Optical Techniques to Characterize Polymer Systems*, H. Bässler and J.-K. Krüger, eds. (Elsevier, Amsterdam, 1989), p. 429.
22. B. A. Auld, *Acoustic fields and waves in solids* (John Wiley, New York, 1973).
23. J. R. Sandercock, "Trends in Brillouin-scattering - Studies of opaque materials, supported films, and cental modes," Top. Appl. Phys. **51**, 173–206 (1982).
24. H. J. Eichler and J. Eichler, *Laser. Bauformen, Strahlführung, Anwendungen* (Springer, Berlin, 2010).
25. M. Mattarelli, M. Vassalli, and S. Caponi, "Relevant Length Scales in Brillouin Imaging of Biomaterials: The Interplay between Phonons Propagation and Light Focalization," ACS Photonics **7**(9), 2319–2328 (2020).